J Biol Inorg Chem (2003) 8: 149–155
DOI 10.1007/s00775-002-0400-0

ORIGINAL ARTICLE

Mei Li · Ming-yih Liu · Jean Le Gall · Lu-lu Gui
Jun Liao · Tao Jiang · Ji-ping Zhang
Dong-cai Liang · Wen-rui Chang

Crystal structure studies on rubrerythrin: enzymatic activity in relation to the zinc movement

Received: 14 May 2002 / Accepted: 25 July 2002 / Published online: 10 September 2002

Abstract Rubrerythrin (Rr) is a non-heme iron protein isolated from anaerobic sulfate-reducing bacteria. Rr is a dimeric molecule, each monomer contains a $Fe(SCys)_4$ center in the C-terminal domain and a binuclear metal center in the N-terminal domain. Rr structures with different protein sources and/or preparation procedures have been studied. Two Rr crystal structures have been solved with significant differences in their binuclear metal centers. The first structure, which was obtained from expressed protein under aerobic conditions, has a diiron–oxo center. The second structure, which was obtained from native protein of *Desulfovibrio vulgaris* under aerobic conditions, has an Fe–Zn center with the zinc position differing from the corresponding iron position in the former structure by approximately 2 Å. The crystal structures of Rr isolated from *D. vulgaris* (Hildenborough, NCIB 8303), the same as the second structured but prepared under anaerobic conditions, are reported in this paper. The binuclear metal center in these structures is an Fe–Zn center. When the crystal was exposed to air, the zinc atom moved gradually, approximately 2 Å, accompanied by the entrance of a water molecule (or hydroxyl group) and changes in the binuclear metal center microenvironment. This finding can explain the differences between the two different structures. The results suggest that the zinc movement may be related to the enzymatic activity of Rr.

Electronic supplementary material is available if you access this article at http://dx.doi.org/10.1007/s00775-002-0400-0. On that page (frame on the left side), a link takes you directly to the supplementary material.

M. Li · L.-l. Gui · J. Liao · T. Jiang · J.-p. Zhang
D.-c. Liang · W.-r. Chang (✉)
National Laboratory of Biomacromolecules,
Institute of Biophysics, Chinese Academy of Sciences,
15 Datun Road, Chaoyang District, Beijing 100101, China
E-mail: wrchang@sun5.ibp.ac.cn
Tel.: +86-10-64888512; Fax: +86-10-64889867

M.-Y. Liu · J. LeGall
Department of Biochemistry and Molecular Biology,
The University of Georgia, Athens, GA 30602-7229, USA

Electronic supplementary material is available if you access this article at http://dx.doi.org/10.1007/s00775-002-0400-0. On that page (frame on the left side), a link takes you directly to the supplementary material.

Keywords Rubrerythrin · Anaerobic · Crystal structure · Iron–zinc center · The zinc movement

Introduction

Rubrerythrin (Rr) is a non-heme iron protein isolated from anaerobic sulfate-reducing bacteria as a homodimer of 44 kDa [1, 2]. Biochemical and spectroscopic studies have shown that Rr contains two domains in one monomer: the C-terminal domain shows the typical sequence features of rubredoxin (Rd), a protein with a non-heme iron center that is also present in some *Desulfovibrio* species, and may also contain a Rd-like $Fe(SCys)_4$ center. The N-terminal domain shows no significant overall homology with that of any other protein, and may contain a binuclear metal center [3, 4].

In 1996, the first Rr structure (model I), which was obtained from expressed protein under aerobic conditions, was solved and revealed the presence of a $Fe(SCys)_4$ center in the C-terminal domain and a diiron–oxo center in the N-terminal domain [5], which was coincident with the early research that each Rr dimer contained six iron atoms [6, 7]. Later, another structure of Rr (model II), which was obtained from native protein under aerobic conditions, was reported [8, 9]. This model had a similar overall structure as model I, but the binuclear metal center was very different, with an Fe–Zn center replacing the diiron center. So there are four iron atoms per dimer in this structure, which is consistent with other research [1, 4]. Moreover, it was striking that the zinc position differed from the corresponding iron position in the first structure by approximately 2 Å.

Apart from the structural difference, the reported enzymatic activity of Rr was diverse. The protein

prepared using different methods may have different dimetal centers, which may result in different activities. For isolated Rr, weak pyrophosphatase activity in vivo was detected [10, 11], but was not confirmed by other laboratories [6, 7]. Rr isolated from *Clostridium perfringens* (another sulfate-reducing bacterium), which had highly homology with Rr from *D. vulgaris*, was detected to have weak superoxide dismutase (SOD) activity [12], but Pierik et al. [7] reported that Rr from *D. vulgaris* had neither SOD nor catalase activity. Later, Geismann et al. [13] proposed that in *C. perfringens*, Rr did not play a role in the defense system against oxygen.

For recombinant Rr, ferrooxidase activity was proposed since Rr was found to be capable of catalyzing oxidation of Fe(II) to Fe(III) in vitro [14]. Also, Rr has been associated with reduced nicotinamide adenine dinucleotide peroxidase activity in vitro [15]. Later, Rd peroxidase activity of Rr was reported by the same laboratory [16].

Here we report the new crystal structures of Rr from *D. vulgaris* and prepared under anaerobic conditions, which may provide some basis for understanding the relationship between its structure and function.

Materials and methods

Protein isolation and crystallization

Isolation and purification of Rr were carried out as previously reported [1], with all procedures under anaerobic conditions. Buffers were first prepared by degassing and then saturating with nitrogen gas. This process was repeated several times. All the purification steps were performed in a Coy anaerobic chamber. Metal contents of the protein were determined by plasma emission analysis. The pyrophosphatase activity was measured as previously described [10].

The crystallization screening was performed as previously reported [5] using the vapor-diffusion method at room temperature under aerobic conditions. Only clustered small crystals were obtained at pH 8.0, so the pH was decreased to 7.0 to obtain large, single crystals. The drops contained Rr protein at a concentration of 10 $mgml^{-1}$, 5% PEG1500, 50 mM Tris-Cl, pH 7.0. The reservoir contained 10% PEG1500 and 100 mM Tris-Cl. After 2–5 days, red-brown crystals with an average size of 0.35×0.3×0.25 mm^3 appeared.

Data collection

Preliminary X-ray crystallographic analysis showed that Rr belonged to space group *I*222. The reflection data were collected by using fresh crystals at room temperature and under aerobic conditions using a Mar Research imaging plate system (diameter 345 mm) at the National Laboratory of Biomacromolecules, Beijing. Two hundred frames were collected with an oscillation angle of 1°. The data was processed and scaled with the DENZO and SCALEPACK [17] programs. Details of the data collection and processing are summarized in Table 1.

Model building and refinement

The two solved Rr structures are referred to as model I (Protein Data Bank, PDB, code 1RYT) [5] and model II (PDB code 1DVB) [9], while our structure of the fresh crystal is referred to as model III. The initial Rr structure of model III was determined using the isomorphous difference Fourier method. Model III was solved using the model I structure with all the metal and solvent molecules removed as the initial model. Model building and refinement were carried out using the TURBO-FRODO [18] and X-PLOR [19] programs on an SGI workstation. After several refinement cycles, the iron atom at the $Fe(SCys)_4$ center was introduced since its electron density behaved well. In addition, the electron density of the dimetal center was also very clear. Then, the iron atom at the dimetal center, which was consistent with the two previously solved structures, was added. Finally, the other metal atom was introduced according to the 2Fo–Fc and Fo–Fc electron density maps. The resolution was gradually extended from 2.7 to 2.5 and 2.2 Å. Finally the individual *B* factors were refined and 70 water

Table 1 Statistics for data collection and refinement of rubrerythrin

	Model III (fresh crystal)	Model IV (3-day-old crystal)	Model V (2-week-old crystal)
Data collection statistics			
Space group	*I*222	*I*222	*I*222
Unit cell dimensions (Å)	$a=49.7$, $b=81.6$, $c=99.8$	$a=50.2$, $b=82.1$, $c=99.9$	$a=50.3$, $b=82.0$, $c=100.0$
Resolution range (Å)	15–2.2	15–2.2	15–2.2
Unique reflections	10,576	10,775	10,827
Multiplicity	11.5	10.4	10.2
Completeness (%) ($I>0\sigma/I>3\sigma$)	99.9/78.1	99.4/77.4	99.9/70.8
R_{merge} (on I)	0.09	0.09	0.11
Refinement statistics			
Number of protein residues in the final model	190	190	190
Number of water molecules	70	65	73
Number of metal atoms	3	3	3
Total number of atoms in the final model	2,079	2,064	2,088
R factor(%)	18.2	19.0	19.3
Initial R_{free}(%)/final R_{free}(%)	28.4/23.1	29.5/24.8	27.8/25.1
Resolution range (Å)	8–2.2	8–2.2	8–2.2
Root-mean-square deviation from ideality			
Bonds (Å)	0.017	0.016	0.016
Angles (°)	2.8	2.6	2.8
Average B factors ($Å^2$)			
Main chain	20.1	20.4	20.4
Side chain	23.0	25.2	24.2
Solvent	34.6	32.7	30.3

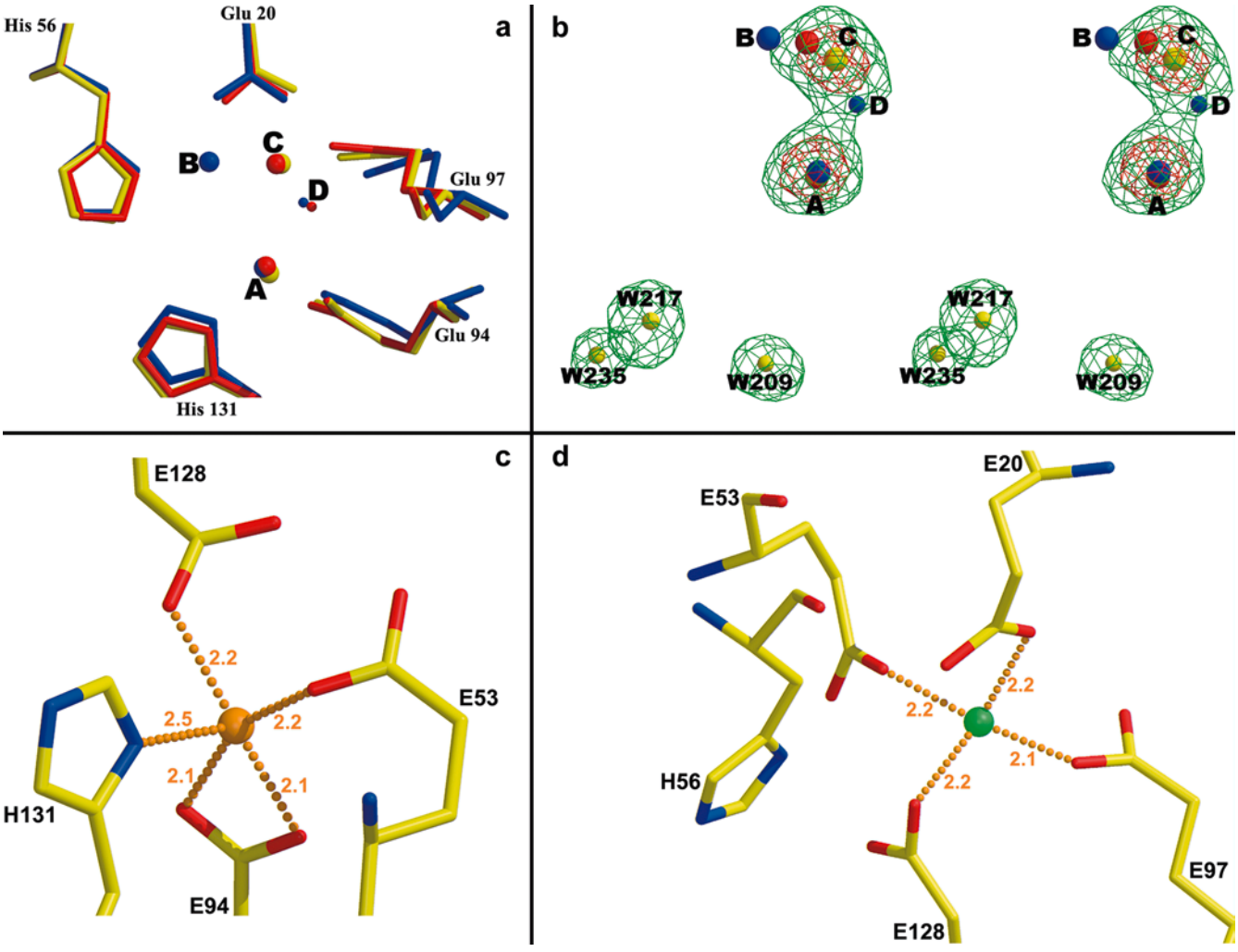

Fig. 1 **a** Superposition of the binuclear metal centers in model I (*red*), model II (*blue*) and model III (*yellow*). The metal atoms are represented as *big spheres* and the water molecules as *small spheres*. In model III, an iron atom is located at site A and a zinc atom at site C (*yellow*). In model I, two iron atoms are located at sites A and C with an oxo bridge at site D (*red*). In model II, an iron atom is located at site A and a zinc atom at site B with a water molecule at site D (*blue*). **b** Stereo view of the omit electron density maps of the binuclear metal center in model III. Fo–Fc maps with metal atoms and water molecules omitted contoured at 3.5σ and 9σ are shown in *green* and *red*. The iron and zinc atoms (*yellow spheres*) are located at sites A and C, respectively. Site D is almost density-vacant at 3.5σ with adjacent water molecules behaving well. To label sites A, B, C and D, the dimetal centers of models III, IV and V were superposed. The metal atoms and water molecules are shown as *yellow spheres* in model III, *red spheres* in model IV and *blue spheres* in model V. **c** Iron-atom coordination of the binuclear metal center in model III. The iron atom is unsaturated octahedrally coordinated with bridging monodentate carboxylates from Glu 53 and Glu 128, bidentate carboxylates from Glu 94, and a histidine ligand of His 131. The iron atom is shown as an *orange sphere*. **d** Zinc-atom coordination of the binuclear metal center in model III. The zinc atom is distorted tetrahedrally coordinated with bridging monodentate carboxylates from Glu 20, Glu 53, Glu 97 and Glu 128. His 56 is not coordinated to the zinc atom at this time. The zinc atom is shown as a *green sphere*

molecules were introduced in batches according to the Fo–Fc and 2Fo–Fc maps. Ten percent of the reflections were set aside to calculate R_{free}. These reflections were included in the final cycles of refinement. More than 90% of the non-glycine residues have the most favored ϕ and ψ angles [20], with no residues having disallowed ϕ and ψ angles in the model III structure. The statistics for the structure are listed in Table 1.

Coordinates

The atomic coordinates (code 1JYB) and structure factors have been deposited in the PDB, Research Collaboratory for Structural Bioinformatics, Rutgers University, New Brunswick, NJ (http://www.rcsb.org/).

Results and discussion

The overall structure and the metal centers in model III

The overall structure of model III is quite similar to the two solved structures in which Rr has two domains. The C-terminal domain contains β-sheets and a $Fe(SCys)_4$ center with two conserved Cys–*X*–*X*–Cys pairs, and all four cysteines (158, 161, 174 and 177) coordinated with

the iron atom in this center, which is similar to Rd [21]. The N-terminal domain contains a four-helix bundle surrounding a binuclear metal center. The structure is similar to other proteins containing diiron sites, such as methane monooxygenase [22, 23] and ribonucleotide reductase R2 [24, 25]. All these proteins have two conserved Glu–*X*–*X*–His pairs, in which the glutamic acid and histidine are all coordinated to the two metals. Similar Glu–*X*–*X*–His pairs (Glu 53, His 56, Glu 128 and His 131) also exist in Rr, but one histidine (His 56) is not coordinated to the dimetal center in model III.

The binuclear metal center of model III was carefully reviewed since the two previously solved structures have distinct dimetal centers. The active centers were labeled as A, B, C and D according to Ref. [8] (Fig. 1a). After several cycles of refinement with the solvent and metal atoms deleted, two metal atoms were introduced according to the 2Fo–Fc and Fo–Fc maps. During refinement, the omit maps were also calculated to check the position of the metal atoms. In these maps, two large peaks were apparent only at sites A and C, indicating the sites of the two metal atoms. Site B was density-vacant, leading to the conclusion that there is no metal atom. Also, there was no obvious density at site D at 3.5σ, with adjacent water molecules behaving well (Fig. 1b). This result indicates that there is no water molecule at the active center in model III, and that the two metal atoms are at sites A and C.

The types of metals in the binuclear metal center were determined with further tests. Fluorescence emission spectrum measurements using the synchrotron radiation source in the Photon Factory (Tsukuba, Japan) detected a prominent peak at the characteristic zinc position, which was evidence of the existence of the zinc atom in the present structure. Plasma emission results also indicated that the sample had both iron and zinc in a proportion of 2:1, which was consistent with the previous result for the sample isolated under aerobic conditions [1]. Since there is a $Fe(SCys)_4$ center in the C-terminal domain, the binuclear metal center of Rr must be an Fe–Zn center.

Although the two solved structures identified that the iron atom was at site A, the ligand coordinations of the atoms at sites A and C were still examined. The atom at site A has an unsaturated octahedral coordination (Fig. 1c), which is close to the characteristic coordination of iron, while site D corresponds to the sixth coordinate position. The atom at site C has a distorted tetrahedral coordination (Fig. 1d), which is similar to that of two other crystal structures containing Fe–Zn centers: purple acid phosphatase (PDB code 1KBP) [26] and calcineurin (PDB code 1AUI) [27]. Therefore, it was concluded that the iron atom is at site A and the zinc atom at site C.

Comparison of the binuclear metal center in models I, II and III

Superposition of the binuclear metal center of the three models is shown in Fig. 1a. The main difference between models II (blue) and III (yellow) is the position of the zinc atom. The zinc atom is at site C in model III, while it is at site B in model II (PDB code 1DVB) [9]. The distance between the two sites is approximately 2 Å, so the ligand coordinations in the two models are slightly different. Glu 97, which forms one of the ligands of the zinc atom in model III (Fig. 1d), is replaced by His 56 in model II. Also, the iron atom in the dimetal center of model II has a saturated octahedral coordination because a water molecule is occupying site D.

The sites of the metals are the same in model III (yellow) and model I (red) (Fig. 1a), but there is a zinc atom at site C in model III, while there is an iron atom in model I (PDB code 1RYT) [5]. In addition, the oxo bridge disappears in model III.

Although the iron in the diiron center could be substituted by zinc in solution, the sample in models II and III is native, namely, isolated from *D. vulgaris*, so zinc incorporation is less likely. In model I, the iron atom might be incorporated to the zinc position after the gene expression procedure [28], as was also noted by Sieker et al. [9].

The zinc movement

Further analysis was needed to understand the significant difference in the zinc positions of models II and III. It was found that their purification procedures were very different with the present sample prepared under

►

Fig. 2 **a** Stereo view of the omit electron density maps of the binuclear metal center in model IV. Fo–Fc maps with metal atoms and water molecules omitted contoured at 3.5σ and 9σ are shown in *green* and *red*, respectively. The iron atom is located at site A; the zinc atom is located at a position between sites B and C. Site D is density-vacant at 3.5σ with adjacent water molecules behaving well. To label sites A, B, C and D, the dimetal centers of models III, IV and V were superposed. The metal atoms and water molecules are shown as *yellow spheres* in model III, *red spheres* in model IV and *blue spheres* in model V, respectively. **b** Coordination of the zinc atom in the binuclear metal center in model IV. The zinc atom is distorted tetrahedrally coordinated with bridging monodentate carboxylates from Glu 53 and Glu 128 and bidentate carboxylates from Glu 20. The ligand bond between the zinc atom and Glu 97 is broken (the distance is 3.1 Å), while the ligand bond between the zinc atom and ND1 of His 56 has not formed yet (the distance is 3.6 Å). The zinc atom is shown as a *green sphere*. **c** Stereo view of the omit electron density maps of the binuclear metal center in model V. Fo–Fc maps with metal atoms and water molecules omitted contoured at 3.5σ and 9σ are shown in *green* and *red*, respectively. The two metal atoms are located at sites A and B. A water molecule or a hydroxyl group with a well-defined map (3.5σ) is located at site D, with adjacent water molecules also behaving well. To label sites A, B, C and D, the dimetal centers of models III, IV and V were superposed. The metal atoms and water molecules are shown as *yellow spheres* in model III, *red spheres* in model IV and *blue spheres* in model V, respectively. **d** Distorted tetrahedral coordination of the zinc atom in the binuclear metal center in model V. The zinc atom is distorted tetrahedrally coordinated with bridging monodentate carboxylates from Glu 20, Glu 53 and Glu 128 and a histidine ligand of His 56. Glu 97 is not coordinated to the zinc atom at this time. The zinc atom is shown as a *green sphere*

anaerobic conditions, while model II was prepared under aerobic conditions [1], so the different zinc position might be caused by the influence of oxygen.

The following experiments were carried out to validate this possibility. Crystals from the same batch (2-day growth period) were selected for time-course experiments. Data were collected for three sets of crystals, including a fresh crystal (data collected right after the crystal appeared), a 3-day-old crystal (data collected 3 days after the crystal appeared) and a 2-week-old crystal (data collected 2 weeks after the crystal appeared). The three Rr structures were solved using model III with all the metal and solvent molecules removed as the initial model. The structure of the fresh crystal was the same as model III with iron at site A, zinc at site C, and nothing at sites B and D (Fig. 1b). The structures of the 3-day-old crystal and the 2-week-old crystal are referred to as models IV and V. The data processing and model refinement procedures of models IV and V were similar to that of model III. The data collection and refinement statistics are summarized in Table 1.

The refined structure using the 3-day-old-crystal data (model IV) has a high density peak at site A, indicating that the iron atom does not move, and has a coordination similar to that of model III. There is also a large peak covering both sites B and C. The 9σ density map shows zinc located between sites B and C. The density is prolonged and its center has a distance of approximately 1 Å from both sites B and C, indicating that the zinc atom is in a transitional state of moving from site C to site B (the temperature factor of the zinc atom is 38.72 Å^2). The 3.5σ density map shows that there is no atom at site D (Fig. 2a). Since the zinc atom moved approximately 1 Å from site C to site B, its coordination with Glu 97 is broken (the distance is 3.1 Å), while the coordination between the zinc atom and ND1 of His 56 has not yet formed (the distance is 3.6 Å) (Fig. 2b).

The refined structure using the 2-week-old-crystal data (model V) has two large peaks at sites A and B indicating two metal atoms at these sites. There is also an electron density peak at site D; this may be a small molecule, like a water molecule or a hydroxyl group (Fig. 2c), which forms a hydrogen bond with Glu 97 and the sixth ligand of the iron atom to saturate its octahedral coordination. The zinc atom has a loose ligand with the ND1 His 56, with a distance of 2.6 Å, and remains

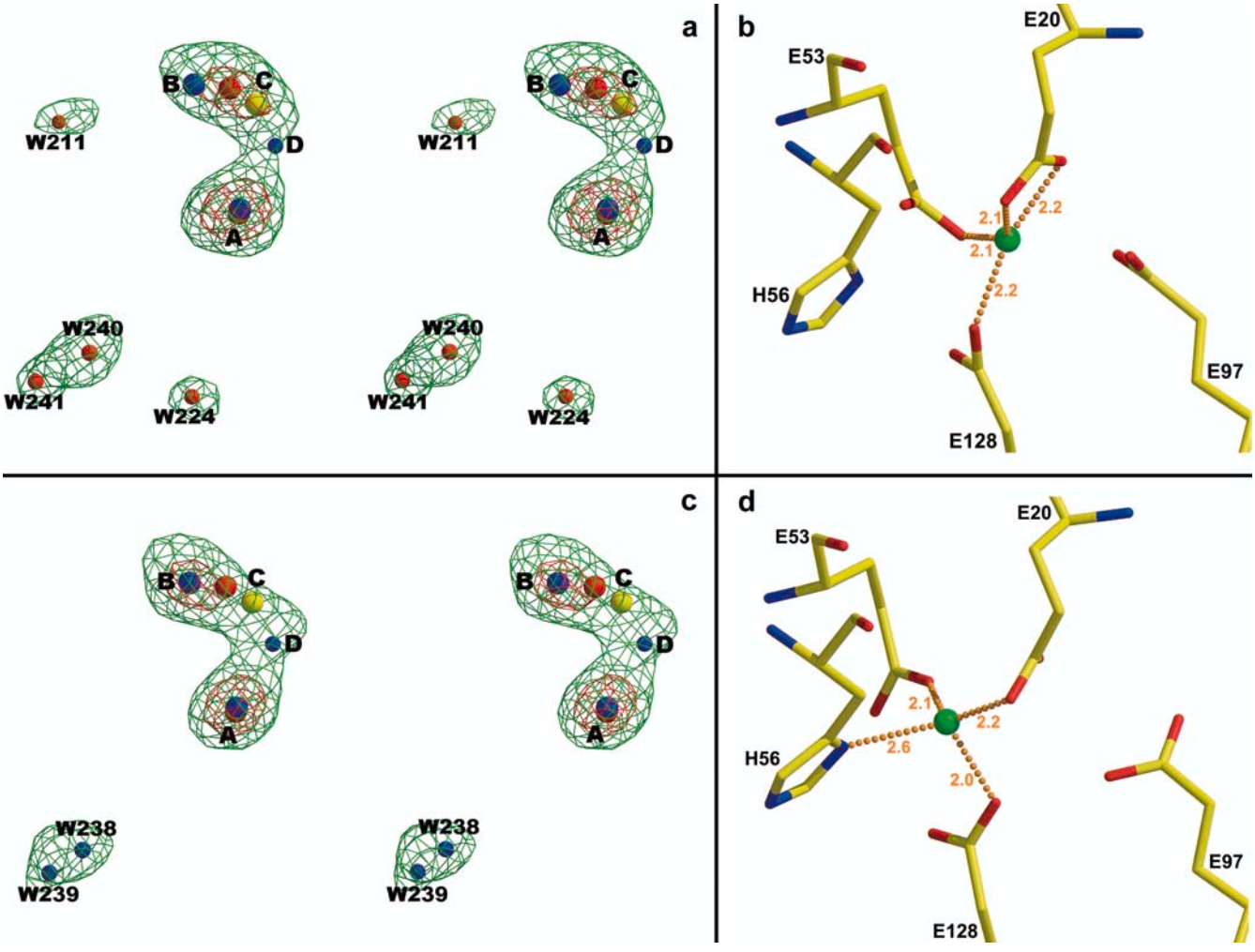

in its tetrahedral coordination (Fig. 2d). The three other ligands of the zinc atom are conserved with slight changes to accommodate the zinc movement, indicating that the binuclear metal center of Rr is highly plastic as was also confirmed for a mutant, E97A of Rr with a diiron center, which also has His 56 as an iron ligand [29]. This high plasticity may be related to its physiological function.

Comparison of the three structures (models III, IV and V) showed that the electron densities of the zinc atom in the three models were very different. The density at site C decreased, while the density at site B increased as the structure changed from model III to model V. There is almost no density change at site A, indicating that the movement of zinc occurs over time.

Biological implications of the zinc movement

Rr has two kinds of dimer formations, known as "head to head" and as "head to tail" [5]. The latter is a more likely the functional form since the distance between the $Fe(SCys)_4$ center and dimetal center, belonging to adjacent monomers, is only about 12 Å; therefore, electron transfer between them is possible. Previous results suggested that His 56 together with Cys 161 of another monomer formed a possible electron-transfer pathway [5]. Another possible pathway was composed of His 131, Gly 162 of another monomer and a water molecule. The C-terminal domain of Rr containing an $Fe(SCys)_4$ center is a Rd-like domain. Since Rd is thought to be an electron-transfer agent [30], the $Fe(SCys)_4$ center may also be an electron-transfer center, while the binuclear metal center may be a catalyzing center in Rr.

Since the zinc movement may be caused by oxygen, we compare the UV–vis spectra of an anaerobically prepared Rr sample both before and after exposure to air. The optical absorptions at 370 and 490 nm of the anaerobic sample were very low, with no visible peaks, indicating that it was in the reduced state. After it was exposed to air, the optical absorptions gradually appeared at 370 and 490nm. Finally, when flashed with oxygen, the ratio of the 370 and 490-nm peaks became consistent with the aerobically prepared Rr sample. This indicates that it has moved to the oxidized state.

The influence of oxygen was also studied by the time-course experiments. Pyrophosphatase activity of Rr samples isolated under anaerobic conditions and exposed to air for 0, 12, 24, 36 and 48 h, respectively, and finally flashed with oxygen, were measured (Table 2). The results showed that reduced Rr is inactive, its pyrophosphatase activity recovered over time, and the oxidized form is fully active, compared to the specific activity of previously reported aerobically prepared sample of Rr [10]. For Rr, the realization of its activity may need the movement of the zinc atom to give sufficient room for substrate binding. Moreover, the zinc movement results in its coordination with His 56 (Fig. 2d), and may force the latter to provide a proton for the reaction. When the zinc atom is at site C (before moving), its distance to ND1 of His 56 is 4.4 Å and the ND1 should be protonated at pH 7; however, it is deprotonated when the zinc atom moves to site B, resulting in a bond between them with a length of 2.6 Å. The lost proton could be transferred to the substrate to carry on the reaction. It was similar to that in glyoxalase II, another type of hydrolase, in which an Fe–Zn center and a "critical histidine" bound to the dimetal center are essential for substrate binding and enzymatic activity [31].

Table 2 Time course of the enzymatic activity of rubrerythrin with oxygen exposure

	Exposure time (h)	Specific activity[a]
Fully reduced	0	17.4
	12	25.2
	24	78.1
	36	117.2
	48	243.5
Fully oxidized	Flashed with O_2	325

[a]One unit of enzyme is the amount necessary to hydrolyze 1 μM pyrophosphate per minute, at 25 °C

However, the question of a hydrolytic function existing under redox control remains unanswered. Pyrophosphate may not be the real physiological substrate for Rr, which is the case for another very active and unrelated pyrophosphatase found in *D. vulgaris* cytoplasm [10].

The zinc movement may explain why Rr has multiple activities, and the biological meaning of the zinc movement may occur in two different ways, one of which causes activation. In the absence of the proper substrate, Rr with the zinc atom at site C exhibits no activity; however, when the substrate binds to the dimetal center and the zinc atom moves, the Rr becomes active. Another possibility is that Rr may have different activities when the zinc atom occupies different positions. The zinc movement may be a functional transformation. In addition, the kind of metal may also influence its activity. The zinc movement procedure (but not iron) which was observed during this research may shed light on the variety and uncertainty of the Rr physiological functions. The zinc movement may also be related to the mechanisms of other enzymes containing binuclear metal centers.

Acknowledgements This project was supported by the Key Project Foundation of the Chinese Academy of Sciences (project no. KJ951-A1-601), the National Key Research Development Project of China (project no. G1999075601) and National Institute of Health Grant GM 56000 (L.G. and M.Y.L.). We thank the Microchemical Analysis Laboratory at the University of Georgia for helping with the plasma emission study on Rr samples.

References

1. LeGall J, Prickril BC, Moura I, Xavier AV, Moura JJG, Huynh B (1988) Biochemistry 27:1636–1642

2. Moura I, Tavares P, Ravi N (1994) Methods Enzymol 243:216–240
3. Ravi N, Prickril BC, Kurtz DM Jr, Huynh BH (1993) Biochemistry 32:8487–8491
4. Prickril BC, Kurtz DM Jr, LeGall J (1991) Biochemistry 30:11118–11123
5. DeMare F, Kurtz DM Jr, Nordlund P (1996) Nature Struct Biol 3:539–546
6. Kurtz DM Jr, Prickril BC (1991) Biochem Biophys Res Commun 181:337–341
7. Pierik AJ, Wolbert RB, Portier GL, Verhagen MF, Hagen WR (1993) Eur J Biochem 212:237–245
8. Sieker LC, Holmes M, LeTrong I, Turley S, Santarsiero BD, Liu MY, LeGall J, Stenkamp RE (1999) Nature Struct Biol 6:308–309
9. Sieker LC, Holmes M, LeTrong I, Turley S, Liu MY, LeGall J, Stenkamp RE (2000) J Biol Inorg Chem 5:505–513
10. Liu MY, LeGall J (1990) Biochem Biophys Res Commun 171:313–318
11. Beeumen JV, Driessche GV, Liu MY, LeGall J (1991) J Biol Chem 266:20645–20653
12. Lehmann Y, Meile L, Teuber M (1996) J Bacteriol 178:7152–7158
13. Geissmann TA, Teuber M, Meile L (1999) J Bacteriol 181:7136–7139
14. Bonomi F, Kurtz DM Jr, Cui X (1996) J Biol Inorg Chem 1:67–72
15. Coulter ED, Shenvi NV, Kurtz DM Jr (1999) Biochem Biophys Res Commun 255:317–323
16. Coulter ED, Kurtz DM Jr (2001) Arch Biochem Biophys 394:76–86
17. Otwinowski Z, Minor W (1997) Methods Enzymol 276:307–326
18. Roussel A, Cambillau C (1991) TURBO-FRODO. Silicon Graphics Applications Directory. Silicon Graphics, Mountain View, Calif
19. Brünger AT (1993) X-PLOR version 31: a system for X-ray crystallography NMR. Yale University Press, New Haven, Conn
20. Ramachandran GN, Sasisekharan V (1968) Adv Protein Chem 23:283–437
21. Eidsness MK, Burden AE, Richie KA, Kurtz DM Jr, Scott RA, Smith ET, Ichiye T, Beard B, Min T, Kang C (1999) Biochemistry 38:14803–14809
22. Rosenzweig AC, Frederick CA, Lippard SJ, Nordlund P (1993) Nature 366:537–543
23. Rosenzweig AC, Nordlund P, Takahara PM, Frederick CA, Lippard SJ (1995) Chem Biol 2:409–418
24. Nordlund P, Sjoberg BM, Eklund H (1990) Nature 345:593–598
25. Nordlund P, Eklund H (1993) J Mol Biol 231:123–164
26. Strater N, Klabunde T, Tucker P, Witzel H, Krebs B (1995) Science 268:1489–1492
27. Kissinger CR, Parge HE, Knighton DR, Lewis CT, Pelletier LA, Tempczyk A, Kalish VJ, Tucker KD, Showalter RE, Moomaw EW, Gastinel LN, Habuka N, Chen X, Maldonado F, Barker JE, Bacquet R, Villafranca JE (1995) Nature 378:641–644
28. Gupta N, Bonomi F, Kurtz DM Jr, Ravi N, Wang DL, Huynh BH (1995) Biochemistry 34:3310–3318
29. DeMare F, Nordlund P, Gupta N, Shenvi NV, Cui X, Kurtz DM Jr (1997) Inorg Chim Acta 263:255–262
30. Sieker LC, Stenkamp RE, LeGall J (1994) Methods Enzymol 243:203–216
31. Zang TM, Hollman DA, Crawford PA, Crowder MW, Makaroff CA (2001) J Biol Chem 276:4788–4795